Monolithic integration of III-V nanowire with photonic crystal microcavity for vertical light emission

Alexandre Larrue,[1] Christophe Wilhelm,[1,2] Gwenaelle Vest,[1] Sylvain Combrié,[3] Alfredo de Rossi,[3] and Cesare Soci[1,2,4,*]

[1]*CINTRA CNRS-NTU-Thales, UMI 3288, Research Techno Plaza, 50 Nanyang Drive, 637553 Singapore*
[2]*Division of Microelectronics, Nanyang Technological University, Block S1, 50 Nanyang Avenue, 639798 Singapore*
[3]*Thales Research and Technology, Route départementale 128, 91767 Palaiseau, France*
[4]*Division of Physics and Applied Physics, Nanyang Technological University, 21 Nanyang Link, 637371 Singapore*
[*] *csoci@ntu.edu.sg*

Abstract: A novel photonic structure formed by the monolithic integration of a vertical III-V nanowire on top of a L3 two-dimensional photonic crystal microcavity is proposed to enhance light emission from the nanowire. The impact on the nanowire spontaneous emission rate is evaluated by calculating the spontaneous emission factor β, and the material gain at threshold is used as a figure of merit of this vertical emitting nanolaser. An optimal design is identified for a GaAs nanowire geometry with r = 155 nm and L~1.1 μm, where minimum gain at threshold ($g_{th} \sim 13\times10^3$ cm^{-1}) and large spontaneous emission factor (β~0.3) are simultaneously achieved. Modification of the directivity of the L3 photonic crystal cavity via the band-folding principle is employed to further optimize the far-field radiation pattern and to increase the directivity of the device. These results lay the foundation for a new approach toward large-scale integration of vertical emitting nanolasers and may enable applications such as intra-chip optical interconnects.

OCIS codes: (350.4238) Nanophotonics and photonic crystals; (160.4236) Nanomaterials; (140.4780) Optical resonators; (140.7270) Vertical emitting lasers.

References and links

1. H. J. Joyce, Q. Gao, H. Hoe Tan, C. Jagadish, Y. Kim, J. Zou, L. M. Smith, H. E. Jackson, J. M. Yarrison-Rice, P. Parkinson, and M. B. Johnston, "III–V semiconductor nanowires for optoelectronic device applications," Prog. Quantum Electron. **35**(2-3), 23–75 (2011).
2. C. Wilhelm, A. Larrue, X. Dai, D. Migas, and C. Soci, "Anisotropic photonic properties of III-V nanowires in the zinc-blende and wurtzite phase," Nanoscale **4**(5), 1446–1454 (2012).
3. W. Wei, X.-Y. Bao, C. Soci, Y. Ding, Z.-L. Wang, and D. Wang, "Direct heteroepitaxy of vertical InAs nanowires on Si substrates for broad band photovoltaics and photodetection," Nano Lett. **9**(8), 2926–2934 (2009).
4. X.-Y. Bao, C. Soci, D. Susac, J. Bratvold, D. P. R. Aplin, W. Wei, C.-Y. Chen, S. A. Dayeh, K. L. Kavanagh, and D. Wang, "Heteroepitaxial growth of vertical GaAs nanowires on Si(111) substrates by metal-organic chemical vapor deposition," Nano Lett. **8**(11), 3755–3760 (2008).
5. K. Tomioka, T. Tanaka, S. Hara, K. Hiruma, and T. Fukui, "III-V nanowires on Si substrate: selective-area growth and device applications," IEEE J. Sel. Top. Quantum Electron. **17**(4), 1112–1129 (2011).
6. A. H. Chin, S. Vaddiraju, A. V. Maslov, C. Z. Ning, M. K. Sunkara, and M. Meyyappan, "Near-infrared semiconductor subwavelength-wire lasers," Appl. Phys. Lett. **88**(16), 163115 (2006).
7. J. C. Johnson, H.-J. Choi, K. P. Knutsen, R. D. Schaller, P. Yang, and R. J. Saykally, "Single gallium nitride nanowire lasers," Nat. Mater. **1**(2), 106–110 (2002).
8. J. C. Johnson, H. Yan, R. D. Schaller, L. H. Haber, R. J. Saykally, and P. Yang, "Single nanowire lasers," J. Phys. Chem. B **105**(46), 11387–11390 (2001).
9. X. Duan, Y. Huang, R. Agarwal, and C. M. Lieber, "Single-nanowire electrically driven lasers," Nature **421**(6920), 241–245 (2003).
10. Y. Xiao, C. Meng, P. Wang, Y. Ye, H. Yu, S. Wang, F. Gu, L. Dai, and L. Tong, "Single-nanowire single-mode laser," Nano Lett. **11**(3), 1122–1126 (2011).

#162603 - $15.00 USD Received 7 Feb 2012; revised 6 Mar 2012; accepted 11 Mar 2012; published 20 Mar 2012

11. B. Hua, J. Motohisa, Y. Kobayashi, S. Hara, and T. Fukui, "Single GaAs/GaAsP coaxial core-shell nanowire lasers," Nano Lett. **9**(1), 112–116 (2009).
12. R. Chen, T.-T. D. Tran, K. W. Ng, W. S. Ko, L. C. Chuang, F. G. Sedgwick, and C. Chang-Hasnain, "Nanolasers grown on silicon," Nat. Photonics **5**(3), 170–175 (2011).
13. C. J. Barrelet, J. Bao, M. Loncar, H.-G. Park, F. Capasso, and C. M. Lieber, "Hybrid single-nanowire photonic crystal and microresonator structures," Nano Lett. **6**(1), 11–15 (2006).
14. H.-G. Park, F. Qian, C. J. Barrelet, and Y. Li, "Microstadium single-nanowire laser," Appl. Phys. Lett. **91**(25), 251115 (2007).
15. S. Noda, M. Fujita, and T. Asano, "Spontaneous-emission control by photonic crystals and nanocavities," Nat. Photonics **1**(8), 449–458 (2007).
16. T. Yoshie, A. Scherer, J. Hendrickson, G. Khitrova, H. M. Gibbs, G. Rupper, C. Ell, O. B. Shchekin, and D. G. Deppe, "Vacuum Rabi splitting with a single quantum dot in a photonic crystal nanocavity," Nature **432**(7014), 200–203 (2004).
17. J. Heo, W. Guo, and P. Bhattacharya, "Monolithic single GaN nanowire laser with photonic crystal microcavity on silicon," Appl. Phys. Lett. **98**(2), 021110 (2011).
18. L. Yang, J. Motohisa, T. Fukui, L. X. Jia, L. Zhang, M. M. Geng, P. Chen, Y. L. Liu, and T. Wang, "Fabry-Pérot microcavity modes observed in the micro-photoluminescence spectra of the single nanowire with InGaAs/GaAs heterostructure," Opt. Express **17**(11), 9337–9346 (2009).
19. C. Z. Ning, "Semiconductor nanolasers," Phys. Status Solidi **247**, 774–788 (2010) (b).
20. M.-K. Seo, J.-K. Yang, K.-Y. Jeong, H.-G. Park, F. Qian, H.-S. Ee, Y.-S. No, and Y.-H. Lee, "Modal characteristics in a single-nanowire cavity with a triangular cross section," Nano Lett. **8**(12), 4534–4538 (2008).
21. A.-L. Henneghien, B. Gayral, Y. Désières, and J.-M. Gérard, "Simulation of waveguiding and emitting properties of semiconductor nanowires with hexagonal or circular sections," J. Opt. Soc. Am. B **26**(12), 2396–2403 (2009).
22. .-Q. Wang, Y.-Z. Huang, Q. Chen, and Z.-P. Cai, "Analysis of mode quality factors and mode reflectivities for nanowire cavity by FDTD technique," IEEE J. Quantum Electron. **42**(2), 146–151 (2006).
23. A. V. Maslov and C. Z. Ning, "Modal properties of semiconductor nanowires for laser application," Proc. SPIE **5349**, 24–30 (2004).
24. I. Friedler, C. Sauvan, J. P. Hugonin, P. Lalanne, J. Claudon, and J. M. Gérard, "Solid-state single photon sources: the nanowire antenna," Opt. Express **17**(4), 2095–2110 (2009).
25. L. Chen and E. Towe, "Nanowire lasers with distributed-Bragg-reflector mirrors," Appl. Phys. Lett. **89**(5), 053125 (2006).
26. L. A. Coldren and S. W. Corzine, *Diode Lasers and Photonic Integrated Circuits* (John Wiley & Sons, New York, 1995).
27. S. Strauf, K. Hennessy, M. T. Rakher, Y. S. Choi, A. Badolato, L. C. Andreani, E. L. Hu, P. M. Petroff, and D. Bouwmeester, "Self-tuned quantum dot gain in photonic crystal lasers," Phys. Rev. Lett. **96**(12), 127404 (2006).
28. Y. S. Choi, M. T. Rakher, K. Hennessy, S. Strauf, A. Badolato, P. M. Petroff, D. Bouwmeester, and E. L. Hu, "Evolution of the onset of coherence in a family of photonic crystal nanolasers," Appl. Phys. Lett. **91**(3), 031108 (2007).
29. T. Baba and D. Sano, "Low-threshold lasing and Purcell effect in microdisk lasers at room temperature," IEEE J. Sel. Top. Quantum Electron. **9**(5), 1340–1346 (2003).
30. R. Hostein, R. Braive, L. Le Gratiet, A. Talneau, G. Beaudoin, I. Robert-Philip, I. Sagnes, and A. Beveratos, "Demonstration of coherent emission from high-β photonic crystal nanolasers at room temperature," Opt. Lett. **35**(8), 1154–1156 (2010).
31. L. C. Andreani, G. Panzarini, and J.-M. Gérard, "Strong-coupling regime for quantum boxes in pillar microcavities: Theory," Phys. Rev. B **60**(19), 13276–13279 (1999).
32. J. M. Gérard, B. Sermage, B. Gayral, B. Legrand, E. Costard, and V. Thierry-Mieg, "Enhanced spontaneous emission by quantum boxes in a monolithic optical microcavity," Phys. Rev. Lett. **81**(5), 1110–1113 (1998).
33. T. Suhr, N. Gregersen, K. Yvind, and J. Mørk, "Modulation response of nanoLEDs and nanolasers exploiting Purcell enhanced spontaneous emission," Opt. Express **18**(11), 11230–11241 (2010).
34. J. M. Gérard, "Solid-state cavity-quantum electrodynamics with self-assembled quantum dots," in *Single quantum dots, Fundamentals, Applications, and New Concepts*, P. Michler, ed. (Springer, Berlin, 2003), pp. 269–314.
35. T. Baba, "Photonic crystals and microdisk cavities based on GaInAsP-InP system," IEEE J. Sel. Top. Quantum Electron. **3**(3), 808–830 (1997).
36. M. Fujita, A. Sakai, and T. Baba, "Ultrasmall and ultralow threshold GaInAsP-InP microdisk injection lasers: design, fabrication, lasing characteristics, and spontaneous emission factor," IEEE J. Sel. Top. Quantum Electron. **5**(3), 673–681 (1999).
37. T. Baba, T. Hamano, F. Koyama, and K. Iga, "Spontaneous emission factor of a microcavity DBR surface-emitting laser," IEEE J. Quantum Electron. **27**(6), 1347–1358 (1991).
38. D. Spirkoska, G. Abstreiter, and A. F. Morral, "GaAs nanowires and related prismatic heterostructures," Semicond. Sci. Technol. **24**(11), 113001 (2009).
39. C. Kim, W. J. Kim, A. Stapleton, J.-R. Cao, J. D. O'Brien, and P. D. Dapkus, "Quality factors in single-defect photonic-crystal lasers with asymmetric cladding layers," J. Opt. Soc. Am. B **19**(8), 1777–1781 (2002).
40. S. Matsuo, A. Shinya, T. Kakitsuka, K. Nozaki, T. Segawa, T. Sato, Y. Kawaguchi, and M. Notomi, "High-speed ultracompact buried heterostructure photonic-crystal laser with 13 fJ of energy consumed per bit transmitted," Nat. Photonics **4**(9), 648–654 (2010).

#162603 - $15.00 USD Received 7 Feb 2012; revised 6 Mar 2012; accepted 11 Mar 2012; published 20 Mar 2012

41. B. Ellis, M. A. Mayer, G. Shambat, T. Sarmiento, J. Harris, E. E. Haller, and J. Vuckovic, "Ultralow-threshold electrically pumped quantum-dot photonic-crystal nanocavity laser," Nat. Photonics **5**(5), 297–300 (2011).
42. C. Sauvan, P. Lalanne, and J. P. Hugonin, "Slow-wave effect and mode-profile matching in photonic crystal microcavities," Phys. Rev. B **71**(16), 165118 (2005).
43. A. R. A. Chalcraft, S. Lam, D. O'Brien, T. F. Krauss, M. Sahin, D. Szymanski, D. Sanvitto, R. Oulton, M. S. Skolnick, A. M. Fox, D. M. Whittaker, H. Y. Liu, and M. Hopkinson, "Mode structure of the L3 photonic crystal cavity," Appl. Phys. Lett. **90**(24), 241117 (2007).
44. A. V. Maslov and C. Z. Ning, "Far-field emission of a semiconductor nanowire laser," Opt. Lett. **29**(6), 572–574 (2004).
45. N.-V.-Q. Tran, S. Combrié, P. Colman, A. De Rossi, and T. Mei, "Vertical high emission in photonic crystal nanocavities by band-folding design," Phys. Rev. B **82**(7), 075120 (2010).
46. J. Vuckovic, M. Loncar, H. Mabuchi, and A. Scherer, "Optimization of the Q factor in photonic crystal microcavities," IEEE J. Quantum Electron. **38**(7), 850–856 (2002).
47. J. Heinrich, A. Huggenberger, T. Heindel, S. Reitzenstein, S. Hofling, L. Worschech, and A. Forchel, "Single photon emission from positioned GaAs/AlGaAs photonic nanowires," Appl. Phys. Lett. **96**(21), 211117 (2010).
48. S. N. Dorenbos, H. Sasakura, M. P. van Kouwen, N. Akopian, S. Adachi, N. Namekata, M. Jo, J. Motohisa, Y. Kobayashi, K. Tomioka, T. Fukui, S. Inoue, H. Kumano, C. M. Natarajan, R. H. Hadfield, T. Zijlstra, T. M. Klapwijk, V. Zwiller, and I. Suemune, "Position controlled nanowires for infrared single photon emission," Appl. Phys. Lett. **97**(17), 171106 (2010).
49. N.-V.-Q. Tran, S. Combrié, and A. De Rossi, "Directive emission from high-Q photonic crystal cavities through band folding," Phys. Rev. B **79**(4), 041101 (2009).

1. Introduction

Quasi-1D semiconductor nanowires have recently aroused much interest as a route to develop novel nanoscale electronic and photonic device concepts. The attention on this emerging class of materials was driven in the early 2000s with the regain of interest in the Vapor-Liquid-Solid (VLS) growth method, which revived the fabrication of 1D nanostructures through different ways of bottom-up guided assembly. Now these methods offer a credible alternative to the traditional top-down approaches for micro/nanofabrication, thanks to the fine control of numerous degrees of freedom achievable during the synthesis, where key structural parameters such as nanowire diameter, length, position, morphology and composition can be adjusted precisely. Significant effort was spent to understand the nanowire growth mechanisms and tune the nanowire optical properties during the synthesis [1,2]. In addition to their excellent structural and optoelectronic properties, nanowires with small cross sectional area allow accommodating lattice strain near the substrate interface, enabling heteroepitaxial growth on highly lattice mismatched substrates [3–5]. Therefore nanowires are widely considered for the design of integrated photonic devices, specifically for the generation and the molding of light at sub-wavelength scales. In this context, single III-V nanowires are particularly suited for the realization of integrated nanoscale light sources emitting in the near or medium infrared spectral range.

Lasing from a single semiconductor nanowire was demonstrated from ultra violet to near infrared wavelengths, under both optical and electrical pumping [6–11]. However, in most cases, studies focused on the emission of single freestanding nanowires removed from their original growth substrate and dispersed horizontally on a host substrate. In this configuration the nanowire acts as the gain medium and, concurrently, its cleaved end facets behave as high crystal quality end mirrors to form an efficient Fabry-Perot cavity. While these structures are suitable for prototyping electrically pumped nanowire lasers, their random positioning on the substrate is a major drawback for large-scale assembly and integration with optical functions. In addition, tuning of the nanowire shape in unconventional geometries is required to achieve single mode operation [10]. Conversely, vertical nanowires can be grown by bottom-up methods at desired locations of the substrate through predefined patterning of the seed catalyst or selective-area growth [5], and their vertical structure makes them natural candidates for surface light emitters. Although in the vertical configuration optical feedback from the facet is severely reduced at the interface with the substrate due to the low refractive index contrast, lasing can still be achieved from nanopillars with sufficiently large diameter [12].

To increase the performance of single nanowire lasers, both theoretical and experimental works have suggested the incorporation of individual nanowires inside a more sophisticated

#162603 - $15.00 USD Received 7 Feb 2012; revised 6 Mar 2012; accepted 11 Mar 2012; published 20 Mar 2012

and efficient optical microcavity to optimize light matter interaction [13,14]. Among the various choices of monolithic optical resonator available, two dimensional photonic crystal (PhC) microcavities with small volume (V) and high quality factor (Q) appear the most suitable architectures to tailor the emission properties of a single emitter placed in the cavity. Up to now, various kinds of low-dimensional nanostructures, such as quantum wells and quantum dots, have been embedded into cavities based on a thin suspended semiconductor membrane with high Q, allowing to access different coupling regimes between active emitters and highly resonant cavity modes [15,16]. In the case of nanowires, the assembly of a single GaN nanowire in a TiO_2 photonic crystal resonator was attempted and led to surface laser emission [17]. Nevertheless, the proposed fabrication scheme is hardly compatible with large-scale integration. Herein we propose to exploit the substantial resonant enhancement induced by the photonic crystal cavity on a single vertical nanowire grown epitaxially on top of the cavity. The ultimate aim is to achieve vertical emitting nanolasers by lowering the lasing threshold through the enhancement of spontaneous emission rate while increasing lasing efficiency by providing a good overlap between the cavity mode and the gain medium. The proposed structure offers a flexible design platform in which the optically active nanomaterial and the microresonator can be engineered independently. Moreover, this architecture is suitable for on-chip, large-scale heterogeneous integration of vertical light sources and is compatible with electrical pumping.

The paper is organized as follows: the properties of a single vertical III-V nanowire cavity are recalled in Section 2, with emphasis on the nanowire geometry required for efficient feedback when considering planar end mirrors. In Section 3, the coupling between a single nanowire and a highly resonant mode of the photonic crystal cavity is described by the spontaneous emission factor of the hybrid cavity mode and the material gain at threshold is introduced as a figure of merit for vertical light emission. The coupling of nanowires with L3 cavities is then discussed in Section 4, and finally in Section 5 the far-field radiation pattern of the coupled microcavity-nanowire structure is considered and optimized by engineering the directivity of the microcavity.

2. The vertical nanowire cavity

For sufficiently large diameters individual freestanding III-V semiconductor nanowires present Fabry-Perot characteristics in micro-photoluminescence experiments [18]. To achieve a vertical nanowire laser, the sub-wavelength waveguide formed by the nanowire body and the end facets must provide an efficient mean to guide and confine photons to form a standing wave in the cavity. The key physical parameters of such resonator are the effective index of guided modes, amplitude reflectivity of the top and bottom mirrors, and indirectly the length of the cavity [19].

The high aspect ratio of III-V nanowires combined with their large refractive index contrast with air allow the existence of guided modes that overlap with the gain medium, a requirement to achieve stimulated emission. The existence of such modes greatly depends on the diameter of the nanowire at the wavelength considered. Optical properties such as reflection coefficient at the facets, confinement and quality factors have been extensively investigated, especially in wide band gap materials since strong confinement of guided modes can be achieved for small diameter nanowires [20–23]. In this work, the focus is on GaAs nanowires and their lower order modes.

#162603 - $15.00 USD Received 7 Feb 2012; revised 6 Mar 2012; accepted 11 Mar 2012; published 20 Mar 2012

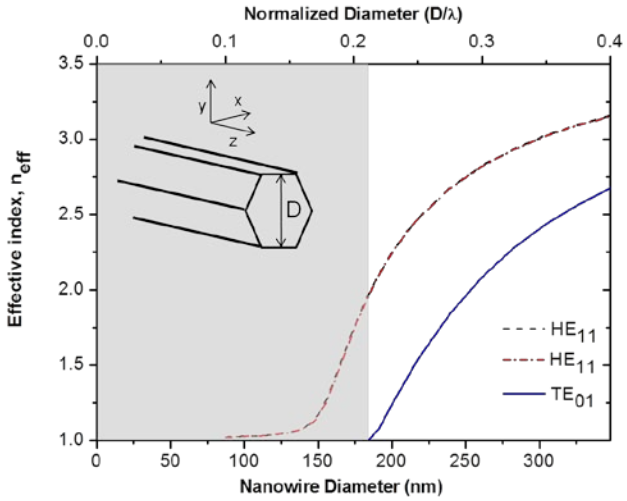

Fig. 1. Effective index of the HE_{11} and TE_{01} propagating modes in an infinitely long GaAs nanowire with hexagonal cross section as a function of the nanowire diameter. The grayed area represents the single-mode guiding regime. The inset shows a schematic of the infinite waveguide.

Figure 1 shows the dispersion relation calculated for the first two guided modes (the fundamental HE_{11} and the first transverse mode TE_{01}) of an infinitely long GaAs nanowire (n = 3.59, λ = 870 nm) as a function of the inner diameter D. Hexagonal cross section is assumed for the waveguide since GaAs nanowires typically crystallize in the zinc blende phase on (111) B oriented surfaces, with hexagonal $(1\bar{1}1)$ or $(11\bar{2})$ side facets [1]. The hexagonal cross section breaks the cylindrical symmetry of the wire and removes the HE_{11} mode degeneracy.

Two distinct regions can be distinguished in Fig. 1. For large diameters (D/λ>0.21), the sub-wavelength waveguide supports multiple modes: fundamental HE_{11} modes as well as higher order transverse modes (for instance TE_{01}). In this case, guided modes are strongly confined inside the wire, thus reducing the propagation losses throughout the cavity and ensuring an efficient overlap with the gain material. Although it is usually better to work with fundamental modes with uniform spatial distribution within the gain material, higher order modes occurring at larger diameters exhibit an electric field profile similar to whispering gallery modes. Such "helicoidally" propagating modes are particularly interesting for vertical nanowire cavities since they are less affected by the low index contrast with the substrate at the bottom mirror, and stimulated emission from these modes has been successfully demonstrated under optical pumping [12].

The second guiding regime occurs at small diameters (D/λ<0.21) where only the quasi-degenerate fundamental HE_{11} modes exist. In this regime guided modes follow closely the light line and start being confined in the wire when D/λ>0.16, however their electric field spreads in the surrounding air. Hence this weak guiding regime imposes stringent constraints on the bottom mirrors to compensate the inherent propagation losses of the mode during a round trip in the cavity. We illustrate this situation by discussing a realistic case. Three dimensional finite-difference time-domain (FDTD) simulations have been carried out to model a vertical GaAs nanowire grown on a non-absorbing substrate at its emission wavelength. Nanowire length of 3 μm, diameter of D = 165 nm and InGaP (n = 3.3) substrate were considered. The low refractive index contrast between the nanowire and the substrate considerably affects reflectance of the bottom mirror (Fig. 2(a)) and, consequently, lowers the quality factor of the resonant mode (Q~50). Design strategies involving metallic and Bragg mirrors were proposed in the literature to increase the reflectivity at the interface with the

#162603 - $15.00 USD Received 7 Feb 2012; revised 6 Mar 2012; accepted 11 Mar 2012; published 20 Mar 2012

substrate [24,25]; in our case the addition of a metallic bottom mirror increases the quality factor of the resonant mode up to Q~150 (Fig. 2(b)). Nevertheless, these strategies require fabrication intensive top-down techniques such as wafer bonding and dry etching and drastically complicate fabrication. More importantly, the approach consisting in the use of a single vertical nanowire as a resonator depends critically on the amount of feedback provided by the nanowire Fabry-Perot cavity, so that performance is limited by intrinsic parameters like nanowire geometry and its refractive index contrast with the surrounding medium (usually air). Thus, thin nanowires with extremely small cross section are unsuitable for the design of a self-consistent cavity.

To reduce the dimensions further and to take full advantage of the controlled synthesis of complex III-V nanowire architectures by bottom-up methods, strategies to increase light-matter interaction with plasmonic resonances or optical microcavities must be employed. Here we consider the assembly of nanowires with high Q photonic crystal cavities.

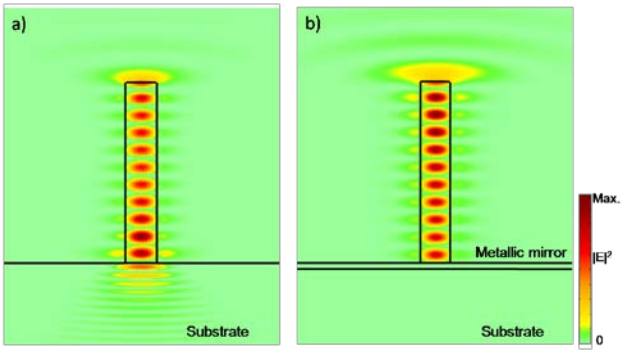

Fig. 2. Electric field intensity of resonant mode in a Fabry-Perot cavity formed by a GaAs nanowire with an InGaP substrate (a) or a 100 nm metallic layer (b) as the bottom mirrors. The nanowire length is L = 3 μm and its inner diameter D = 165 nm.

3. Coupling of a vertical nanowire with a photonic crystal microcavity

One of the consequences of assembling a vertical nanowire on top of a photonic crystal cavity is the modification of its spontaneous emission due to the coupling with a small-volume and high-Q cavity mode. This is an attractive perspective for the realization of nanolasers with low threshold, large modulation bandwidth and low-power consumption. The redistribution of the spontaneous emission rate is quantified by the spontaneous emission factor β, which defines the ratio between the spontaneous emission rate of the resonant mode and the spontaneous emission rate into all the other modes. In waveguide laser diodes β typically ranges from ~10^{-5} to 10^{-4} [26]; β factors approaching unity were obtained at low temperature in small volume photonic crystal microcavities embedding InAs quantum dots [27,28], while β as large as 0.1 were demonstrated at room temperature in microdisks with quantum well active media or photonic crystal lasers with InAsP quantum dots [29,30]. The enhancement of the spontaneous emission (Purcell effect) is also related to the spontaneous emission factor. Although in semiconductors the Purcell effect is well understood for point-like emitters with narrow spectral linewidth, e.g. quantum dots at low temperature [31,32], the interaction of a microcavity with any light emitting material is expected to induce a modification of its spontaneous emission. A model for the calculation of the Purcell enhancement in the general case of spectrally broad emitters was proposed by Suhr *et al.* [33]. In general $\beta = F/(F+\gamma)$, where γ is the ratio of the emission into all the modes but the cavity mode of interest, normalized to the emission without the cavity (the "natural" radiative lifetime) [34]. Therefore the spontaneous emission factor is a good gauge for the dynamics of the nanowire-PhC structure. For an active material with Lorentzian spectral broadening, β is given by [35,36]:

#162603 - $15.00 USD Received 7 Feb 2012; revised 6 Mar 2012; accepted 11 Mar 2012; published 20 Mar 2012

$$\beta = \frac{p\Gamma_r \lambda^3}{4\pi^2 n_{eq}^3 V_{eff}} \frac{\lambda}{\Delta\lambda} \tag{1}$$

where the cavity volume has been replaced by the mode volume V_{eff}, p is a factor denoting the polarization anisotropy of the spontaneous emission of the dipole emitter, Γ_r the relative confinement factor, n_{eq} the equivalent refractive index of the laser mode, and λ and $\Delta\lambda$ are the central wavelength and width of the spontaneous emission spectrum. Notice that in this expression it is assumed that the total emission energy equals that in free space; although this assumption is appropriate for the nanowires considered in this study, it may not hold for emission spectra with narrow linewidth [37]. The relative confinement factor Γ_r is related to the optical confinement factor Γ by [35]:

$$\Gamma = \frac{n_{NW}^2 V_{NW}}{n_{eq}^2 V_{eff}} \Gamma_r \tag{2}$$

Here n_{NW} and V_{NW} represent the refractive index and the volume of the nanowire active material. In our geometry, light matter interaction occurs in the region where the electric field of the optical mode supported by the coupled cavity system overlaps with the nanowire gain medium. Therefore, the optical confinement factor Γ is expressed by the overlap integral:

$$\Gamma = \frac{\iiint_{NW} \varepsilon(\vec{r}) \left| \boldsymbol{E}(\vec{r}) \right|^2 dr^3}{\iiint_{Tot} \varepsilon(\vec{r}) \left| \boldsymbol{E}(\vec{r}) \right|^2 dr^3} \tag{3}$$

Substituting Γ_r in Eq. (1), the spontaneous emission factor of the coupled nanowire-PhC structure becomes:

$$\beta = \frac{p\Gamma \lambda^3}{4\pi^2 n_{NW}^2 n_{eq} V_{NW}} \frac{\lambda}{\Delta\lambda} \tag{4}$$

Note that β is inversely proportional to the mode volume $V_{eff} = V_{NW} / \Gamma$ of the coupled system. Hereafter the GaAs nanowire will be considered as a gain medium with spectrally broad photoluminescence. At cryogenic temperature, the spectral broadening of its spontaneous emission is approximately ΔE = 6 meV (the photon energy being E = 1.51 eV), which corresponds to $\lambda/\Delta\lambda$~250 [38]. Since nanowires with wurtzite crystallographic phase display a strong emission anisotropy and the relative small aspect ratio (L<1.2 μm) limits the form birefringence [2], one can assume p = 1 for the polarization anisotropy. Moreover, the equivalent refractive index of the lasing mode is close to the refractive index of the nanowire gain medium, and $n_{NW}^2 n_{eq}$ can be numerically approximated by n_{NW}^3.

While β describes the spontaneous emission rate redistribution into the laser mode, stimulated emission is characterized by the modal gain. The gain that the material has to provide to compensate the optical losses of the cavity, or material gain at threshold (g_{th}), can be derived equating the rate of stimulated emission $\tau_{st}^{-1} = g\Gamma c / n$ to the cavity lifetime ω_0 / Q, where g is the material gain, c the speed of light, n the refractive index of the gain medium, ω_0 the resonant frequency of the mode, and Q the quality factor of the overall structure entailing the photonic crystal cavity and the vertical nanowire [39]:

$$g_{th} = \frac{n\omega_0}{c} \frac{1}{\Gamma Q} \tag{5}$$

In the next section we consider a well-known L3 photonic crystal coupled to a vertical GaAs nanowire and evaluate the dependence of the spontaneous emission factor and the material gain at threshold on nanowire geometry.

#162603 - $15.00 USD Received 7 Feb 2012; revised 6 Mar 2012; accepted 11 Mar 2012; published 20 Mar 2012

4. Vertical GaAs nanowire coupled to the L3 PhC microcavity

Two-dimensional photonic crystal cavities are known for their ability to confine light into a very small volume. This unique feature allows tailoring the emission properties of solid-state emitters located inside the cavity, which can ultimately lead to the development of ultra-low threshold lasers and quantum cavity electrodynamics [16,40,41]. Here we focus on the well-characterized L3 cavity, which consists of a small line defect cavity formed by the omission of three-in-line holes in the ΓK direction of an hexagonal photonic crystal lattice with lattice constant a and hole radius r = 0.29a. The photonic crystal slab comprises of an InGaP film (n = 3.3) with a thickness of h = 0.64a, and the two holes terminating the cavity in the ΓK direction are shifted by a displacement s = 0.18a. This results in a quality factor of ~40000 for the TE-like fundamental resonant mode (Fig. 3) [42]. The choice of the L3 design is motivated by the spatial distribution of the cavity mode with a maximum of intensity in the center of the resonator, which favors the coupling with the nanowire by mode matching selection. In addition the L3 cavity offers high discrimination between the resonant modes due to optical losses [43]. Adding a nanowire on top of the air-bridged PhC at an anti-node of the electric field intensity is expected to break the symmetry of the slab structure and to lower the quality factor of the fundamental mode by increasing out of plane losses.

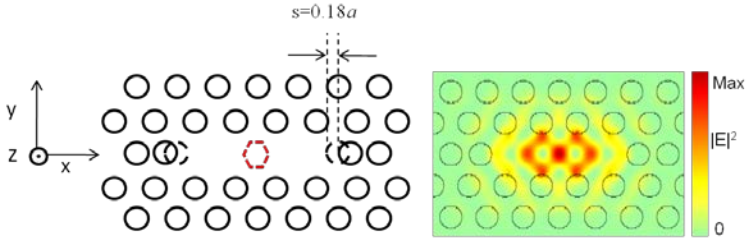

Fig. 3. (Left) Schematic of the modified L3 photonic crystal cavity. The dashed red hexagon illustrates the position of the vertical nanowire on top of the photonic crystal slab. (Right) Electric field intensity distribution of the fundamental resonant mode of the bare L3 cavity.

FDTD simulations are carried out to determine the resonant mode properties (β and g_{th}) of the nanowire-PhC structure by evaluating the overall quality factor Q and the overlap integral Γ as a function of nanowire radius and length. The results of these calculations, where a mesh of 20 points per lattice constant a was used to discretize the calculation domain and the boundary conditions were perfectly matched layers, are shown in Fig. 4. Depending on the nanowire diameter, two regimes are clearly distinguished. In general, the presence of the vertical nanowire perturbs the resonant mode of the PhC and degrades its quality factor (Fig. 4(a)). However, for very thin nanowires (i.e. for radii r<0.25a), the Q factor decreases monotonically with the increase of nanowire radius but remains larger than ~1000 (with the exception of specific lengths that are discussed below). For large nanowire radii (i.e. r>0.25a), the generalized quality factor drops to values below 1000. On the other hand, the overlap integral Γ is small for thin nanowires (Γ~0.5x10^{-3}) and increases by two orders of magnitude for the largest nanowire radii (Fig. 4(b)). The spontaneous emission factor β results from the balance between the overlap integral and the volume of the gain medium: in the small radii regime, β ranges from 0.007 to 0.09 as a function of nanowire length, while for large radii values as high as 0.3 can be achieved (Fig. 4(c)). In general, the nanowire length has limited effect on the quality factor and the overlap integral, with the exception of specific lengths that correspond to multiples of the half wavelength of the guided mode with effective index n_{eff} ($L = \lambda/2n_{eff}$) in the Fabry-Perot nanowire cavity. When the PhC and the native nanowire cavity modes are in resonance out of plane losses increase and the overall quality factor is substantially reduced. The gain at threshold presents local maxima for the resonance lengths due to the simultaneous reduction of Q and Γ (Fig. 4(d)). These lengths should then be avoided for optimal laser operation, hence precise control of nanowire length during the

#162603 - $15.00 USD Received 7 Feb 2012; revised 6 Mar 2012; accepted 11 Mar 2012; published 20 Mar 2012

synthesis is quite critical. The gain at threshold ranges between $\sim 13\times10^3$ and 80×10^3 cm^{-1}; due to the large overlap with active medium the minimum value of g_{th} is achieved for the larger nanowire volume. Although these values seem rather high, an optical gain of $g=13\times10^3$ cm^{-1} has already been reported for a GaN nanowire coupled to a TiO_2 PhC cavity under optical pumping [17].

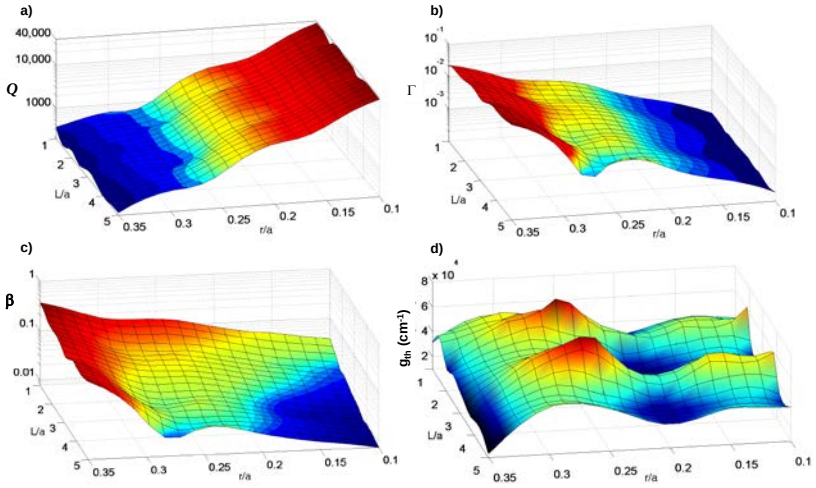

Fig. 4. Dependence of the overall quality factor Q (a), the overlap integral Γ of the cavity mode with the nanowire (b), the spontaneous emission factor β (c), and the gain at threshold g_{th} (d) on nanowire radius and length.

The representative coupling regimes between the vertical nanowire and the PhC membrane are illustrated in Fig. 5. The intensity distribution of the near-field shows that at small radii (Figs. 5(a) and 5(b)), the electric field of the cavity mode is mainly confined in the slab and spreads weakly into the nanowire, while at optimum coupling (Fig. 5(c)) guided modes are allowed to propagate and the nanowire acts as a funnel for photons extracting light vertically. In k-space, the nanowire modifies the electric field profile of the resonant mode by increasing the overlap with the light cone region (Figs. 5(d)-5(f)). Consequently, the high Q mode is more vulnerable to the coupling with radiative modes and its Q factor decreases.

Based on the above discussion, the optimal design of the coupled structure consists of a nanowire with L = 5a and r = 0.35a where large spontaneous emission factor (β~0.3) and minimum gain at threshold ($g_{th}\sim 13\times10^3$ cm^{-1}) are simultaneously achieved. This regime is particularly interesting for lasing since the electric field is not only localized at the base of the nanowire but propagates in the gain region with a shape similar to longitudinal modes of the nanowire Fabry-Perot cavity. Compared to a single vertical nanowire standing on the substrate, this configuration presents a double advantage. First, the photonic crystal cavity prevents photons from escaping at the bottom, recycling them inside the gain region. The efficiency of this process is superior to a standard nanowire cavity (the overall quality factor is Q ~200, larger than in the structure displayed in Fig. 2(a)) and the photonic crystal cavity acts as a reservoir for photons. More importantly, the PhC forces single-mode selection.

#162603 - $15.00 USD Received 7 Feb 2012; revised 6 Mar 2012; accepted 11 Mar 2012; published 20 Mar 2012

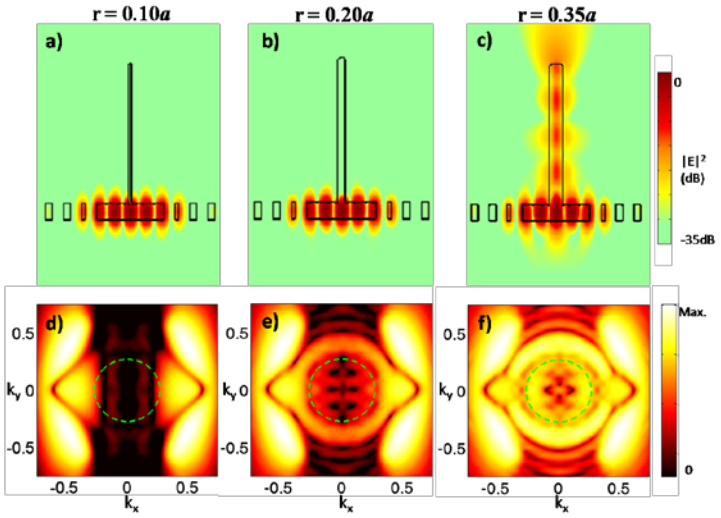

Fig. 5. Side view of the electric field intensity ($|E|^2$) distribution and Fourier transform of the electric field just above the photonic crystal membrane. The nanowire dimensions are r = 0.10*a* and L = 5*a* (a,d), r = 0.20*a* and L = 5*a* (b,e), r = 0.35*a* and L = 5*a* (c,f). The dashed green circles in (d-f) represent the cross section of the light cone.

5. Directivity of the nanowire-PhC system

In view of all optical signal processing, a key feature of vertical emitting light sources is directivity. Indeed, it is highly desirable to control the shape of the vertical beam to optimize collection efficiency of the emitted light within objective lenses or single-mode optical fibers, or to collimate the optical signal on photoreceivers in optical interconnects. Nanowire-PhC structures offer several degrees of freedom for engineering the far field distribution compared to individual vertical nanowires. Maslov *et al.* have demonstrated that the emission distribution of a single vertical nanowire is highly dependent on guided mode geometries and optimal directionality can be achieved only for HE_{11} modes [44]. Moreover, for small diameters the emission properties of individual nanowires are complicated by the anisotropy induced by dielectric effects and light diffraction [2]. To elucidate these issues, we have calculated the far-field distribution patterns for the nanowire-PhC structure with the smallest volume nanowire (r = 0.1*a*, L = *a*), a nanowire with average dynamic characteristics (r = 0.2*a*, L = *a*), and the optimal nanowire (r = 0.35*a*, L = 5*a*) and the results are shown in Fig. 6 [45,46]. The addition of nanowires perturbs the angular distribution of the far-field emission of the bare L3 cavity (Fig. 6(a)). As the diameter of the nanowire increases, the divergence of the beam decreases (Fig. 6(b)-6(d)). The best directivity is obtained for the optimized coupled structure (r = 0.35*a* L = 5*a*, Fig. 6(d)), where the overlap of the bare L3 cavity mode with the HE_{11} nanowire mode is maximum. As a result, ~66% of the total emission from the lasing mode of the nanowire PhC structure could be collected with an objective lens with numerical aperture of NA = 0.4.

Of further fundamental interest would be taking advantage of site-controlled nanowire growth to implement a self-aligned quantum dot inside the wire, whereby single photon sources could be developed by growing the quantum dot in a small volume nanowire and in the proximity of the PhC membrane [47,48]. In this configuration, the relevant parameters that characterize the interaction of the cavity mode with the quantum dot are the Purcell and quality factors of the coupled system. For example, for a nanowire with r = 10*a* and L = *a* with an ideal GaAs quantum dot embedded 80 nm above the PhC membrane (e.g. a small nanowire region surrounded by axial AlGaAs barriers), the Purcell factor would be F_p~2. This configuration, however, would suffer from poor directivity (Fig. 6(b)). Fortunately this issue can be overcome using the strategy proposed in refs [45,49], where “band folding” is induced

#162603 - $15.00 USD Received 7 Feb 2012; revised 6 Mar 2012; accepted 11 Mar 2012; published 20 Mar 2012

by a subharmonic modulation of the air-holes size around the cavity. This modification affects the electric field distribution of the resonant mode in the reciprocal space and folds a fraction of the field to the center of the first Brillouin zone, thus improving directionality of the emission. Figure 7 shows the effects of this modification on the far-field distribution of the nanowire-PhC structure where the air hole size around the L3 cavity is modulated periodically by $\Delta r = \pm 0.01a$, while the two terminal holes in the ΓK direction are still shifted by a displacement $s = 0.18a$.

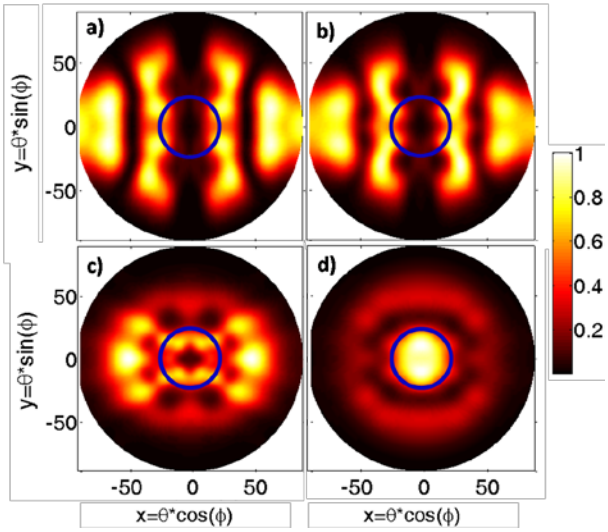

Fig. 6. Far-field radiation pattern of the bare L3 cavity (a), and the L3 cavity with a nanowire on top (c-d). The corresponding nanowire dimensions are: $r = 0.10a$ and $L = a$ (b), $r = 0.20a$ and $L = a$ (c), and $r = 0.35a$ and $L = 5a$ (d). The solid blue circle represents the ideal collection angle of an objective with numerical aperture of 0.4.

The far-field distribution pattern of the modified L3 cavity (Fig. 7(a)) and the nanowire-PhC structures with small nanowire volume (Figs. 7(b)-7(c)) change radically compared to the unmodified cavity design and their vertical directivity is significantly improved. For coupled structures with nanowire dimensions of $r = 0.10a$, $L = a$ and $r = 0.20a$, $L = a$ the collection efficiency of the mode of interest (i.e. the fraction of light emitted from this mode collected with an objective with numerical aperture NA = 0.4) increases from 16% to 74% and from 32% to 56%, respectively. Such improvement is due to the modification of the spatial profile of the electric field in the vicinity of the PhC which spreads weakly into the nanowire. In these cases, the main contribution in the calculation of the retarded potential is given by the cavity and the nanowire can be considered as a weak perturbation. Nevertheless, the improvement in directivity is associated to an increase of out of plane losses that degrades the quality factor. For the nanowire with the smallest volume, Q drops from 35800 to 28000 and consequently the Purcell factor decreases slightly to $F_p \sim 1.5$. For the optimal geometry ($r = 0.35a$, $L = 5a$) the far-field radiation pattern does not change significantly upon modification of the L3 cavity (Fig. 7(b)). This is not surprising since emission depends primarily on the electromagnetic field components of the mode guided into the nanowire.

#162603 - $15.00 USD Received 7 Feb 2012; revised 6 Mar 2012; accepted 11 Mar 2012; published 20 Mar 2012

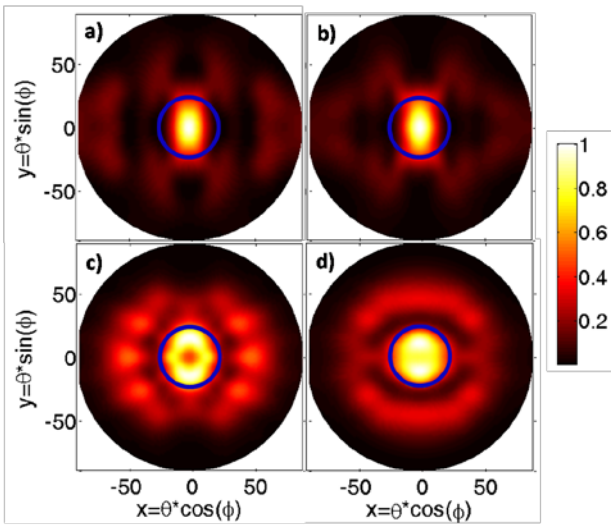

Fig. 7. Far Field radiation pattern of the bare modified L3 cavity alone (a), and the modified L3 cavity with a nanowire on top (c-d). The corresponding nanowire dimensions are: r = 0.10*a* and L = *a* (b) r = 0.20*a* and L = *a*(c) and r = 0.35*a* and L = 5*a* (d). The solid blue circle represents the ideal collection angle of an objective with numerical aperture of 0.4.

Conclusions

An original architecture consisting of a vertical III-V nanowire grown in the antinode of a resonant photonic crystal cavity mode is proposed to realize vertical emitting nanolasers with high efficiency and low lasing threshold. The coupling regimes of this coupled structure were characterized by mapping the overall quality factor and the overlap integral as a function of nanowire diameter and length. These quantities allow evaluating the spontaneous emission factor of the resonant mode of the nanowire-PhC structure and estimating the gain at threshold: the former quantifies the redistribution of the spontaneous emission rate into the lasing mode, while the latter is used as a figure of merit for stimulated emission. Table 1 summarizes the characteristics of the coupled systems investigated. For the nanowire-PhC structures based on the L3 cavity, the optimal nanowire geometry corresponds to r = 0.35*a* and L = 5*a* (for GaAs r = 155 nm and L~1.1 μm) where a minimum gain at threshold ($g_{th} \sim 13 \times 10^3$ cm^{-1}) and large spontaneous emission factor (β~0.3) are simultaneously achieved. Modification of the L3 photonic crystal cavity based on the band folding principle can be used to increase the overall directivity of the vertical emitting coupled system with small diameter nanowires. Compared to photonic crystal lasers incorporating quantum dots as active material in the PhC membrane and depending on the coupling regime exploited, the proposed architecture allows taking advantage of the larger gain volume of the active material or to enhance the spontaneous emission rate and improve light extraction of a quantum dot grown within a small nanowire. Moreover, these structures offer greater flexibility in controlling light-matter interaction, and are compatible with large scale integration and electrical pumping schemes, thus could enable new approaches for the realization of nanoscale light sources and optical interconnects.

#162603 - $15.00 USD Received 7 Feb 2012; revised 6 Mar 2012; accepted 11 Mar 2012; published 20 Mar 2012

Table 1. Characteristics of the nanowire-PhC structure

Nanowire dimensions in the coupled structure	g_{th} (cm^{-1})	β	F_p	Collection efficiency*	Beam directivity
Standard L3 PhC cavity					
r = 0.10a, L = a	$37x10^3$	0.03	2	16%	Low
r = 0.20a, L = a	$30x10^3$	0.08	-	32%	Low
r = 0.35a, L = 5a	$13x10^3$	0.30	-	66%	High
Optimized L3 PhC cavity					
r = 0.10a, L = a	$48x10^3$	0.03	1.5	74%	High
r = 0.20a, L = a	$32x10^3$	0.08	-	56%	Medium
r = 0.35a, L = 5a	$13x10^3$	0.32	-	63%	High

*The collection efficiency is defined as the percentage of emission from the nanowire-PhC structure lasing mode collected with an ideal objective with a numerical aperture of NA = 0.4.

Acknowledgments

The authors are grateful to Dr. N.V.Q. Tran for his help in developing the code for the calculation of far field patterns. This work was financially supported by the NTU NAP startup grant M58110065, the MERLION Programme 2010 of the French Embassy in Singapore (dossier 2.04.10), and the Funding of Initiatives in Support of NTU 2015 (M58110092). C.W. gratefully acknowledges the joint PhD program between the Nanyang Technological University and ParisTech.

#162603 - $15.00 USD Received 7 Feb 2012; revised 6 Mar 2012; accepted 11 Mar 2012; published 20 Mar 2012